BJR https://doi.org/10.1259/bjr.20160906

Received: 1 December 2016 | Revised: 15 March 2017 | Accepted: 30 March 2017

Cite this article as:
Wiggins CJ, Schäfer A, Dhital B, Le Bihan D, Turner R. After over 200 years, 7 T magnetic resonance imaging reveals the foliate structure of the human corpus callosum *in vivo*. *Br J Radiol* 2017; **90**: 20160906.

FULL PAPER

After over 200 years, 7 T magnetic resonance imaging reveals the foliate structure of the human corpus callosum *in vivo*

[1]CHRISTOPHER J WIGGINS, PhD, [2,3]ANDREAS SCHÄFER, PhD, [4]BIBEK DHITAL, PhD, [5]DENIS LE BIHAN, MD, PhD and [3,6,7]ROBERT TURNER, PhD

[1]Scannexus BV, Maastricht, Netherlands
[2]Department of Neurophysics, Max Planck Institute for Human Cognitive and Brain Sciences, Leipzig, Germany
[3]Siemens Healthcare GmbH, Diagnostic Imaging, Magnetic Resonance, Erlangen, Germany
[4]Department of Radiology—Medical Physics, University Medical Center, Freiburg, Germany
[5]NeuroSpin, Joliot Institute, CEA-Saclay Center, Gif-sur-Yvette, France
[6]University of Amsterdam Faculty of Medicine (AMC-UvA), Amsterdam, Netherlands
[7]Department of Physics, University of Nottingham, Nottingham, UK

Address correspondence to: Dr Christopher John Wiggins
E-mail: *cjwiggins@gmail.com*

Objective: A fine structure of the corpus callosum (CC), consisting of radial lines, is seen in historical anatomical atlases as far back as that of Vicq d'Azyr (1786). This study examines a similar pattern observed *in vivo* using high-resolution MR images at 7 T.
Methods: 8 healthy subjects were examined with 7.0-T MRI. Anatomical images were collected with a gradient echo scan with 0.5-mm isotropic resolution, which were rated for visibility of the radial pattern. In addition, the second eigenvector of the diffusion tensor images was examined.
Results: The fine radial lines are detected not only in the sagittal view but also in the axial view of the *in vivo* MR images. From this, it is likely that these structures are two-dimensional ribbons. Interestingly, and confirming the structural nature of these stripes, the second eigenvector of the diffusion tensor imaging data shows an extremely similar pattern of oriented foliate structure. A similar modular structure involving transient septa has been observed previously in histological sections of human fetal CC.
Conclusion: The separate sets of data—the atlas of Klingler, anatomical images and second eigenvector images—all indicate a ribbon-like arrangement of the fibres in the CC. As such, they closely match the structures shown in the drawn atlases of as old as 1786.
Advances in knowledge: This ribbon arrangement of fibres in the CC, previously unseen in CT or lower field MRI, can now be observed *in vivo*. This appears to match over two centuries of *ex vivo* observations.

INTRODUCTION

In vivo biomedical imaging techniques have been constantly evolving, with both new methods being developed as well as significant improvements made to existing technology. In the latter case in particular, it is worth reflecting whether these advances can lead to the ability to discern aspects of human anatomy that have previously been either unobserved or only observable in *ex vivo* preparations. As an example of this, we examine the details of the human corpus callosum (CC).

The CC is the major white matter fibre tract connecting the cerebral hemispheres of vertebrate brains. It has a clear role in interhemispheric communication, carrying the overwhelming majority of interhemispheric communications. It is a unique and heavily myelinated structure. Dissection, histological staining and diffusion MRI confirm that the predominant fibre orientation within this structure is transverse.

In histological sections of human fetal CC,[1,2] a modular structure involving transient septa has been observed. This suggests an importance of these structures in normal brain development. As yet, these structures have not been appreciated and their importance has been overlooked clinically, despite evidence that the CC continues to develop through adulthood.[3–6] This is perhaps because, at clinical field strengths, MRI (as well as other anatomic imaging modalities such as CT and positron emission tomography) shows no finer structure within the CC. Human brain studies of the modularity of the CC have so far revealed only gross distinctions along the anteroposterior axis, between segments connecting homologous brain areas. In particular, Hofer and Frahm[7] have used diffusion tensor imaging (DTI) to segment

the CC using four vertical partitions, relative to the connections between specific cortical areas. They mention, however, that their mapping of parietal, temporal and occipital fibre bundles overlap, and these are therefore all grouped together into a fifth, most posterior segment. Other groups have attempted to differentiate regions of the CC based on measurements of axonal diameter.[8–10]

Keeping the septa described above in mind, a review of older, hand-drawn atlases reveals that the CC is frequently depicted in sagittal section with its volume shaded with radial lines. Figure 1 shows four representative atlases, those of d'Azyr from 1786,[11] Bell from 1802,[12] Dejerine and Dejerine-Klumpke from 1895[13] and Gray from 1918.[14]

When photographic brain atlases such as Schaltenbrand and Wahren[15] are examined, a finer structure can also be observed. On sagittal sections, a faint pattern of radial lines can be seen on the CC. These faint lines might initially be assumed to be from

Figure 1. Four representative figures from historical, drawn atlases: upper left—d'Azyr (1786),[11] upper right—Bell[12] (1802), lower left—Dejerine and Dejerine-Klumpke (1895)[13] and lower right—Gray (1918).[14] Of note is the consistent depiction of the corpus callosum, which is shaded using radial lines in every case (insets at centre). While this might be considered as artistic licence, the repetitive use of the same shading motif over more than a century is remarkable. Comparison with *in vivo* atlases such as those shown in Figure 2 removes all doubt that these shadings are related to structures observed by the anatomists at the time that the atlases were created.

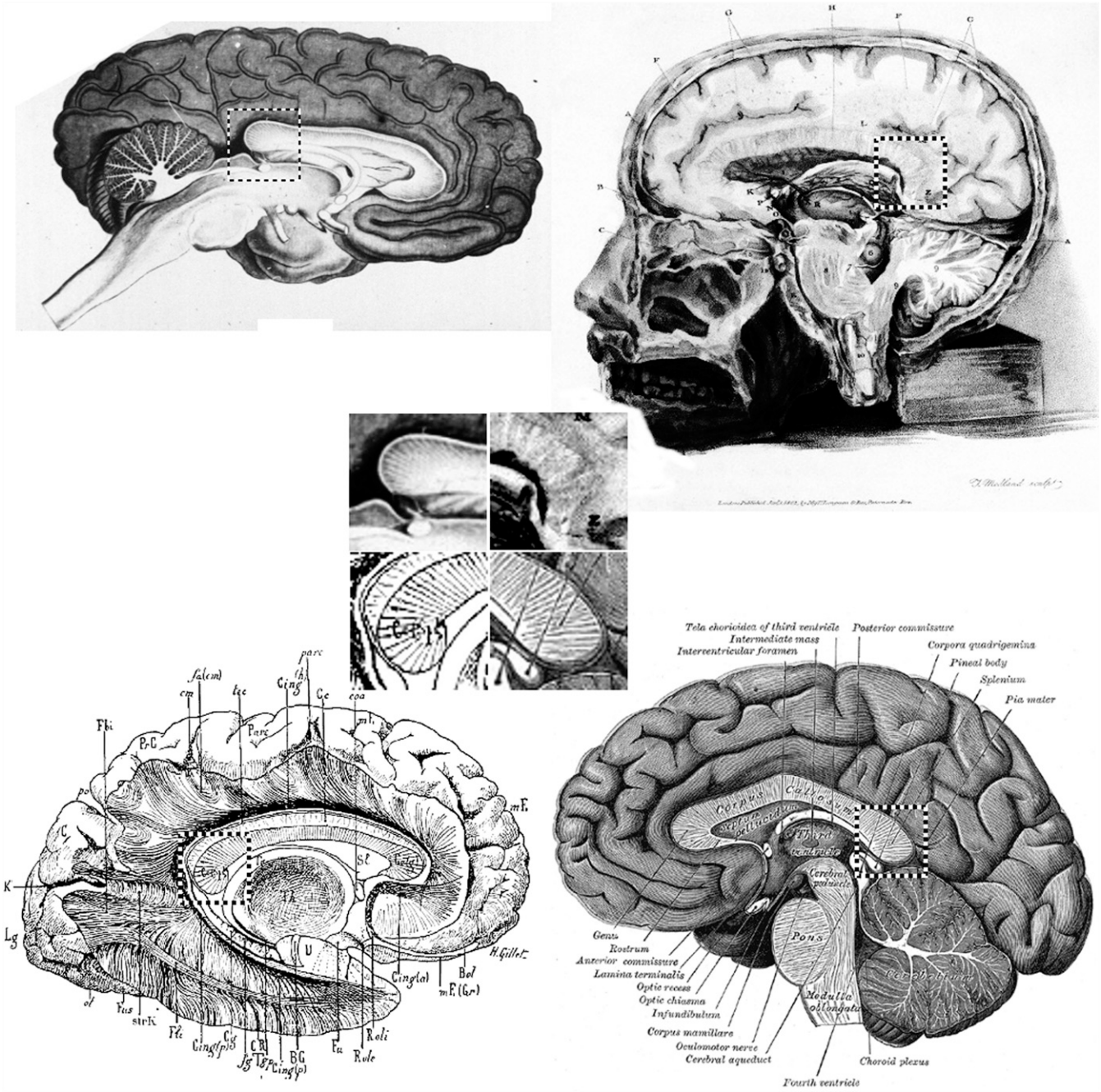

Figure 2. Comparison of the *ex vivo* preparation (left) of Ludwig and Klingler[16] (reproduced with kind permission from S. Karger AG, Basel) with 7.0-T gradient echo magnitude (upper right) and phase (lower right) MRI data. The laminar structure of the corpus callosum is clearly visible in the photograph and a similar pattern appears in the MR images.

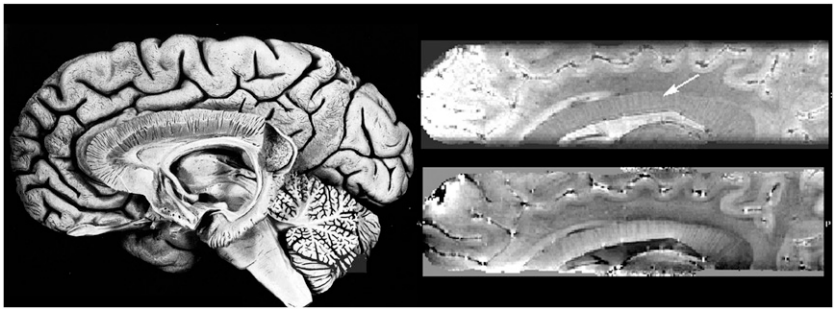

microvasculature. However, examination of the coronal sections from this same reference shows such lines also in the anterior and posterior sections of the CC, where they run horizontally. Unfortunately, the absence in this atlas of transverse sections at this level prevents complete visualization of these structures. Even more strikingly, preparations of *ex vivo* samples designed to separate fibre bundles, such as those shown in the atlas of Ludwig and Klingler,[16] show distinctly that there is an arrangement of flat sheets, containing nerve fibre bundles, which are stacked in the anteroposterior direction. A clear example of this is show in tabula 71 from this atlas, which is reproduced as Figure 2 alongside 7.0-T MR images acquired with the same protocol that will be used in this study. The radially arranged, laminar structure of the CC is well presented in this photograph of a prepared brain. (As will be detailed later, a similar pattern is seen on the MR images.) It is thus clear that the depiction of radial lines on the early drawn atlases is due to the familiarity of the anatomists with this structure in *ex vivo* preparations.

It is now established beyond doubt that the increase in spin magnetization produced by higher static magnetic fields in MRI can give a corresponding increase in the signal-to-noise ratio (SNR) of the resulting images. This enables the use of considerably higher spatial resolution, giving scan times of under 10 min for 500 micron isotropic resolution with good SNR over an entire *in vivo* human brain. While much of the work to date has concentrated on newly important contrast mechanisms such as phase contrast,[17] and the orientation of tissue relative to the applied field,[19] images of animal brain[20] and human brain[21] have shown a spectacular gain in observable structural detail, such as cortical layers.[22] Fine details such as the Virchow–Robin spaces can also be observed in the white matter.[23] Such anatomical details have previously been observed easily only on *ex vivo* dissections.

Using Ultra High Field (UHF) MRI, we here demonstrate *in vivo* imaging of foliated structure of the CC, comprising sheets of transcallosal axons located roughly perpendicular to the superior and inferior surfaces of this structure. Two MRI methods were used, gradient echo and DTI.

Gradient echo imaging[24] is, in a magnitude reconstruction, sensitive to the local inhomogeneity of the magnetic field, mainly caused by susceptibility differences between different structures or tissues. Particularly with UHF MRI, it has allowed extremely high-resolution images of the human brain to be acquired.[25] In addition, information from the phase signal, which is sensitive to offsets in the magnetic field, has been used both as a way of delineating blood vessels such as veins[26] and as a source of more general image contrast in itself.[17,18] From the latter, techniques to map the susceptibility of tissues have been developed.[27]

DTI[28] is used routinely to investigate white matter fibre orientation. DTI models as a tensor the self-diffusion of water molecules in the white matter. In white matter bundles without crossing fibres, the primary eigenvector of this tensor has been shown to correspond well to axonal orientation. The CC meets this criterion. In the CC, the fractional anisotropy is very high, and the primary eigenvector runs transversely, as expected. It is generally believed that most of the water MRI signal giving signal in DTI comes from within axons. Since axons are roughly cylindrical, diffusion along the other two perpendicular directions, *i.e.* dorsal–ventral and anteroposterior, is expected to be similar.[29]

METHODS AND MATERIALS

MR system

A 7.0-T MRI system (Siemens Medical Solutions, Erlangen, Germany) was used with a 24-channel phased-array radiofrequency coil (Nova Medical, Wilmington, MA) This system has a maximum gradient strength of 70 mT m^{-1} with slew rate 200 mT m^{-1} s.

Subjects

The data of eight healthy subjects (three males and five females, 20–29 years) were acquired after signed written consent.

Three-dimensional Fast Low Angle Shot (FLASH) images

Data acquisition

T_2* weighted images were acquired. A fully flow compensated three-dimensional spoiled gradient echo sequence was used. Image resolution was set to 0.5 mm isotropic, matrix size 336 (phase) × 384 (read) with 72 slices (12 % oversampling). A repetition time of 42 ms, echo time = 25 ms and a flip angle of 12° were used. The acquisition bandwidth was set to 50 Hz/pixel. The total imaging time was 18 min 51 s.

Data processing

The magnitude images were not processed further. However, unprocessed phase images suffer from aliasing owing to the

background field inhomogeneities, and therefore these low-spatial frequency variations need to be removed. For this study, processing consisted of first a convolution of the complex data with a Gaussian kernel. The raw complex data were then divided by this convolved version and the phase was then computed. Two kernel sizes of 10 and 20 pixels full width at half maximum (FWHM) were used for comparison of the quality of the resulting images. The final result is a high-pass filtered phase image, preserving anatomical detail.

Image grading

In order to judge the visibility of these structures, as well as the relative benefit of the two kernel sizes, two scorers rated the data independently. The two scorers were PhD physicists with extensive experience in *in vivo* MRI, with over 20 years' experience in neurological MRI. For a given subject, all three versions (magnitude, phase with 10 pixel FWHM and phase with 20 pixel FWHM) were presented at the same time. The visibility of the apparent stripes within the CC was scored according to the following scheme, in which the term "half" is in reference to anteroposterior length of CC:

0—no visual signs of a fine structure

1—only visible in very limited region (less than half, only unilaterally)

2—visible in a limited region (more than half unilaterally or less than half bilaterally)

3—visible in a very extensive region (complete unilateral or more than half bilaterally)

4—completely visible bilaterally.

For each data set, all three sets of images were examined magnitude, *i.e.* T_2*, "phase10" (10 pixel FWHM processing) and "phase20" (20 pixel FWHM processing). Scorers were also asked to judge which of the three images they preferred, on the basis of observability of the striped pattern in the CC, for a given subject.

Diffusion tensor images

Data acquisition

The sequence used a stimulated echo with fat suppression. The diffusion-weighting scheme used a *b*-value of 75 s/mm^2 in 60 directions with 1 repetition, as well as a *b*-value of 1500 s mm^{-2} in 60 directions with 3 repetitions. 30 slices (field of view 200 × 200 mm, matrix size 144 × 144, slice thickness 1.4 mm) were acquired using an echoplanar imaging readout, repetition time = 6 s, echo time = 42 ms, delta = 110.5 ms, parallel imaging (iPAT) factor 3 for a total of roughly 24 min of scanning. The acquisition bandwidth was set to 1530 Hz/pixel.

Diffusion tensor imaging processing

Data were corrected for motion using the FLIRT algorithm and FSL tools (http://www.fmrib.ox.ac.uk/fsl/) followed by noise correction[30] and calculation of the diffusion tensor. As will be discussed in the results section, only the second eigenvector is of further interest in this study. The orientation of the second eigenvector was then spatially mapped, to investigate its correlation with local brain structure. Owing to apparently corrupt data, one data set could not be analyzed; so, only the DTI data from seven subjects are presented.

Analysis of lamina orientation

In order to compare the data between subjects, 3 × 3 × 3 pixel volumes of interest (VOIs) were selected in three regions of the CC, one posterior (*i.e.* centred in the splenium), one anterior (*i.e.* centred in the genu) and one at the midpoint. The midpoint VOI was centred in the anteroposterior direction at a point halfway between the anterior and exterior extents (along the midline) of the CC and in the inferosuperior direction at a point between the upper and lower surfaces. The average vector was then calculated for each subject in each of the three positions.

Since the main structure observed in both T_2* images and second eigenvector DTI is a radially oriented laminar structure in the sagittal plane, the initial analysis consisted of the calculation of the deviation of the DTI vectors from an superoinferior direction. In order to normalize for individual head position, the angular difference between the middle VOI and either the anterior or posterior VOIs was calculated and compared.

RESULTS

The high-resolution three-dimensional, T_2* weighted as well as phase images indeed show the CC not as a homogeneous white matter body, but also reveal "stripes" along the callosal body that have a distinct similarity to the laminar structures seen in *ex vivo* preparations (Figure 2). In the gradient echo images (Figure 3), the stripes show alternating higher and lower intensity, suggesting localized changes in water concentration or T_2*. In axial view (Figure 3b,e), these stripes extend left to right along the axonal direction, whereas in the sagittal view they span the CC, running perpendicular to its dorsal and ventral surfaces (Figure 3c,f). Since the stripes do not lie along the intersection of the orthogonal imaging planes, they themselves must represent planar structures. By this argument, their shape cannot easily be attributed to simple linear structures, as one might expect from isolated blood vessels. While in principle, a collection of small (below the imaging resolution) blood vessels, packed tightly in a plane, could create such a pattern, this would seem unlikely, especially owing to lack of appearance of the necessary supplying or draining blood vessels. In addition, the diffusion encoding of the DTI data should be sufficient to fully crush the signal from moving blood, and so it should not be contributing to the DTI data. Even if such an arrangement of blood vessels were to exist, then this would result in planar spaces between the planes of blood vessels. In the end, the appearance is best explained as arising from quasi-two-dimensional planar structures forming septa that separate planes of axons passing transversely across the CC.

The visibility of these stripes was assessed by taking the median values of the ratings, resulting in values of 2.5 (magnitude), 4 ("phase10") and 3 ("phase20"). Graders generally preferred the "phase10" images (in all cases except one in which one reviewer preferred "phase20"). This result suggests that this structure could be seen in an extensive region (complete unilateral or more than half bilaterally) regardless of the type of image.

As a distinct method to confirm this apparent structure, we examined the DTI data from the CC. Owing to the strong dominance of the primary eigenvector in the left–right direction, if there were no planar structure the second eigenvector would have no preferential orientation. It also follows that the third eigenvector provides no further information, since it is by definition orthogonal to both the first and second. On this basis, maps of the second eigenvector were examined for apparent structure, particularly in the sagittal plane (Figure 4). These data show, remarkably, that diffusion in the anteroposterior direction is markedly more hindered than in the dorsal–ventral direction. In addition, the data show that the second and third eigenvectors are not of similar magnitude, which would result in a random orientation of these vectors. This directional bias cannot be attributed to water molecules within the cylindrically symmetric axons. It can arise only from tissue water occupying some other asymmetric, oriented structures present in the CC.

It is important to note here that what is being examined is the second eigenvector, and not the first eigenvector. The fanning out of the nerve fibre bundles as they exit the CC might be thought to cause a similar pattern to be shown in a projection of the first eigenvectors onto the sagittal plane. However, since we are looking at the second (and not at a projection of the first) eigenvector, this cannot explain the result.

To give a measure of comparison between subjects, the calculated angular differences from midpoint to genu and from midpoint to splenium are presented in Table 1. To measure statistical significance, the data were subjected to a non-parametric permutation analysis with the null hypothesis that there was no difference in measured angle between the midpoint and genu or—separately—between midpoint and splenium. 10,000 permutations of the values were used in each case. The observed results were then compared with these distributions in order to generate p-values. The data show that the second eigenvectors are significantly inclined in the genu ($p = 0.031$) and splenium ($p = 0.046$) compared with those at the midpoint. This is to such an extent as to be nearly perpendicular compared with the data from the midpoint.

DISCUSSION

This is the first reported investigation of the small-scale modular septated structure of CC in living adult human brain. These structures are easily visible in high-field, high-resolution MR images and have confirmatory evidence from DTI. The knowledge and ability to directly image this structure, even without significant post-processing, is potentially relevant to a variety of studies, including brain development, large-scale white matter structure and structural–functional correlations of callosal regions. In addition, the DTI results give insights into the role of extra-axonal water. Clinically, the ability to visualize this fine structure enables measurement of its properties (integrity of folia, changes in folia dimensions etc.) and their relationship with disease and disease progression.

This asymmetry in the second and third eigenvectors has previously been noted.[31,32] Atkinson et al[33] have previously used this information to also attribute a ribbon-like structure to the CC, as well as to reference an apparent directional structure in the electron micrographs published by Aboitiz et al.[34] However, it would appear that this suggested structure has not been widely recognized in the field, and it can be hoped that the additional verification that the 7.0-T MRI brings to this will help to spread this concept.

Brain development

The work by Jovanov-Milosevic et al[1,2] clearly demonstrates the existence of septa within the prenatal brain. This modular organization of the CC is undoubtedly crucial in brain development.[35] The glial matrix acts to guide axonal fibres to their destinations. While this matrix is believed to vanish with later development, within the CC traces of this matrix appear to persist into adulthood and may provide the MR contrast pattern reported here. It is unclear whether this pattern is actually some vestige of the glial matrix which is organizing the nerve fibres into sheets, or simply a remaining organization of the fibres after the matrix has vanished. The authors of this present work are not aware of any evidence from histology of such a remaining physical matrix, and so suggest the latter as the most likely explanation.

Figure 3. From left to right, magnitude, "phase10" and "phase20" images from a gradient echo acquisition, with, from top to bottom, sagittal, axial and coronal views through the three-dimensional data set. Of note is the striped appearance of the corpus callosum on the sagittal and axial views (arrows). FWHM, full width at half maximum.

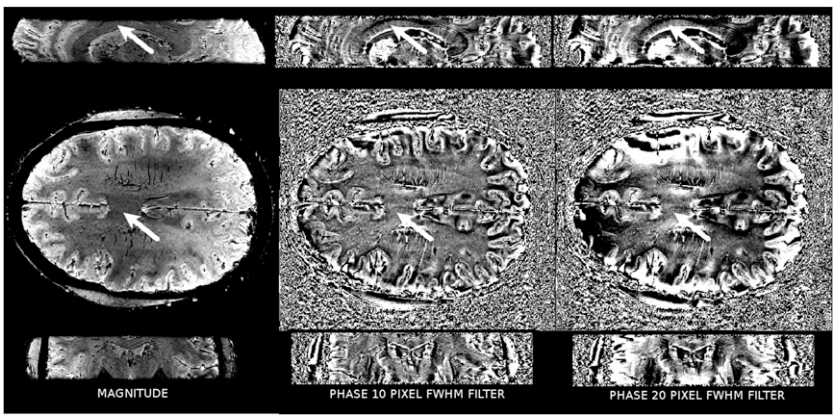

Figure 4. Sagittal view of the second eigenvector of diffusion tensor imaging data: of note is the radial pattern in the corpus callosum, matching that seen in the structural images. Since the primary diffusion direction is known to follow the axons that run between the hemispheres, *i.e.* through the plane of the image, this indicates that there must be planar structures. In addition, the third eigenvector provides no additional information, as it will be perpendicular to the first and second, and so is effectively this same image with the vectors rotated by 90 degrees.

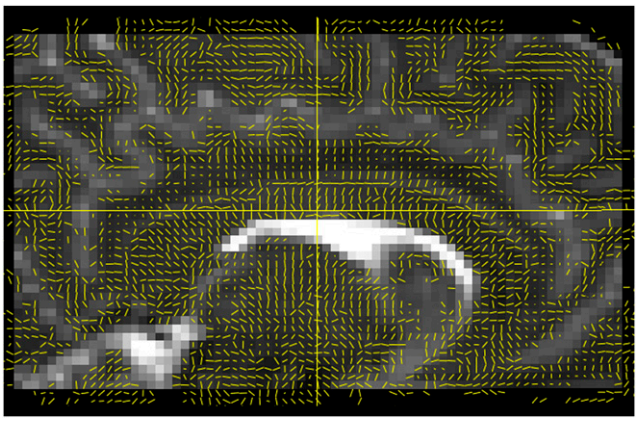

The CC has also been reported to develop through adulthood.[3–6] The ability to examine the internal structure of the CC *in vivo* may thus provide additional measures to track these developments. While this might be considered a confound in this present study, the narrow age range of the subjects (less than a decade) combined with their ages (between 20 and 30 years, which is a relatively stable period in changes to CC anatomy)[4–6] should minimize any age-related contribution to these data. In addition, some studies have shown differences in CC microstructure related to cognitive ability.[36] If such microstructure differences are related to differences in laminar structure, such differences might be directly observable with techniques such as those used in this study.

Large-scale white matter structure

In general, the regions of the cortex and their connections through regions of the CC show a similar geometrical arrangement, with anterior regions of the cortex connecting through anterior regions of the CC.[37–39] This implies, and DTI tractography has shown, that there is relatively little cross-over of fibre bundles between the CC and cortical areas. It has been suggested theoretically that cortical connections are made most efficiently by means of sheet-like structures.[40] The linear arrangement of ocular dominance columns[41] also suggests a foliate packing arrangement of axons as the optic radiation arrives at the primary visual cortex. Recent work using advanced diffusion acquisition and analysis techniques has indicated that cortico–cortical pathways form in parallel sheets.[42] This raises the interesting possibility that the laminar structure we have observed within the CC might persist all the way to the cortex. Further work would be needed to confirm this, possibly from more targeted MR examinations or with the use of the higher contrast and SNR expected from the next generation of MRI scanners with higher field strengths (*e.g.* 9.4 T, 10.5 T and 11.7 T). However, such confirmation will certainly be complicated by the frequent crossings of fibre tracts that do not traverse the CC.

Structural–functional correlations of callosal regions

In general, the CC has no obvious internal anatomical landmarks. Even the features seen in this study show little variation along the CC. Many researchers have attempted to define subdivisions of the CC, based either on vertical partitions[7,39,43] or on equal angular sectors relative to the callosal centroid.[44–46] Interestingly, much of the work using DTI tractography[7,43] has used the vertical partition scheme, whereas the angular sector scheme has generally been used merely as a convenient method to parcellate the CC, but without a direct apparent anatomical basis. With the knowledge that the CC actually exhibits such an approximately angulated structure, additional insight can be obtained into the subdivisions of the CC. For instance, what Hofer and Frahm[7] denoted as a fifth, most posterior segment is an area where the observed structure of the CC is effectively horizontal. If the septations that are present in prenatal development have a role in guiding fibres between similar cortical areas, it is thus unsurprising that an arbitrary vertical segmentation may result in regions containing fibre bundles from different regions. Referring to Figure 2 of this reference, it is clear that it would be more correct to divide the fifth segment into at

Table 1. Analysis of diffusion tensor imaging second eigenvectors in the sagittal plane

Subject	Midpoint–genu angle (degrees)	Midpoint–splenium angle (degrees)
1	94	−52
2	99	−79
3	55	−76
4	94	−123
5	128	−55
6	81	−74
7	124	−110
Average	96.4 ± 24.9	−81.3 ± 26.5

3 × 3 × 3 pixel volumes of interest were averaged as described in the text. A non-parametric permutation analysis showed that the second eigenvectors are significantly inclined in the genu ($p = 0.031$) and splenium ($p = 0.046$) compared with those at the midpoint.

Figure 5. Modification to the segmentation scheme of Hofer and Frahm[7] (right), where the most posterior segment, V, can be divided into at least two if not three subsegments along a horizontal line, with parietal connections (VI) inferior to this line, occipital (V) below and temporal lying along the line itself, resulting in a proposed new segmentation scheme.

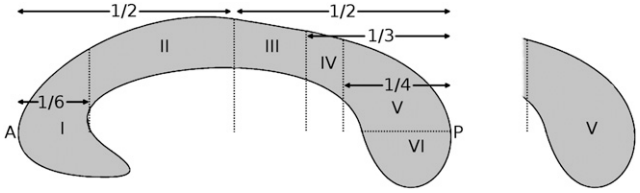

least two if not three subsegments along a horizontal line, with parietal connections inferior to this line, occipital below and temporal lying along the line itself, resulting in a proposed new segmentation scheme (Figure 5).

Thus, an additional prospect is the use of the observed foliation as a basis for parcellation of the CC. Because this structure can be visualized *in vivo*, it could be incorporated into parcellation strategies based on a particular individual anatomy, rather than arbitrary vertical or angular partitions. Furthermore, the foliation might be useful as a powerful constraint on MR tractography of transcallosal fibre bundles.

Axonal diameter mapping and dispersion

A growing field of work is the attempts to map axonal diameters.[8–10] Recently, attempts have been made to correctly account for directional dispersion during such studies.[47] In such studies, the possible dispersion is usually considered as being cylindrically symmetric. This leads to a possible conflict of such models with the laminar structure observed. It is possible, however, that the spatial scales of the laminar structures and the axonal dispersion are sufficiently different that, on a local scale, a cylindrical model is indeed appropriate. Further study is clearly necessary to determine whether these laminar structures have an impact on axonal diameter mapping methods.

Role of non-axonal water in diffusion tensor imaging

This work also provides evidence of the important contribution of non-axonal water to DTI data, presumably mostly located within glial cells. Prior to this study, diffusion MRI measurements in white matter so far have been concerned with fibre orientation, fibre density and primary diffusion direction. However, it appears that additional structural information may be inferred from DTI data. Further work is required to examine such contributions.

Limitations

While it is clear from these results that 7.0-T MRI can provide image details that are starting to rival *ex vivo* preparations, some limitations do exist. First, at present, the availability of 7.0 T is limited, and at the time of writing no clinically certified systems exist, which limits the applicability in a hospital setting. This is set to change, however, as at least one manufacture has announced plans to deliver certified 7.0-T systems in 2017. Secondly, while this study has observed the stripes over a significant portion of the CC, they are not always observed over the entire length. Further optimization of the imaging parameters may help resolve this, or perhaps a change to yet higher field systems (*e.g.* 9.4-T, 10.5-T or the planned 11.7-T systems). Third, a high image resolution is required to observe this pattern, which might be problematic in patient populations where subject motion compliance may be limiting.

CONCLUSION

The use of cutting edge MRI techniques, such as the high-resolution gradient echo imaging at 7.0 T and DTI data presented here, has been shown to enable the *in vivo* study of structure within the CC that has only been seen hitherto in *ex vivo* and histological studies. The ability to directly visualize such structures *in vivo* has significant potential to advance research into several aspects of normal and pathological brain architecture.

REFERENCES

1. Jovanov-Milosevic N, Benjak V, Kostovic I. Transient cellular structures in developing corpus callosum of the human brain. *Coll Antropol* 2006; **30**: 375–81.
2. Jovanov-Milosevic N, Culjat M, Kostovic I. Growth of the human corpus callosum: modular and laminar morphogenetic zones. *Front Neuroanat* 2009; **3**: 6. doi: https://doi.org/10.3389/neuro.05.006.2009
3. Pujol J, Vendrell P, Junque C, Marti-Vilalta JL, Capdevila A. When does human brain development end? Evidence of corpus callosum growth up to adulthood. *Ann Neurol* 1993; **34**: 71–5. doi: https://doi.org/10.1002/ana.410340113
4. McLaughlin NC, Paul RH, Grieve SM, Williams LM, Laidlaw D, DiCarlo M, et al. Diffusion tensor imaging of the corpus callosum: a cross-sectional study across the lifespan. *Int J Dev Neurosci* 2007; **25**: 215–21. doi: https://doi.org/10.1016/j.ijdevneu.2007.03.008
5. Hasan KM, Kamali A, Iftikhar A, Kramer LA, Papanicolaou AC, Fletcher JM, et al. Diffusion tensor tractography quantification of the human corpus callosum fiber pathways across the lifespan. *Brain Res* 2009; **1249**: 91–100. doi: https://doi.org/10.1016/j.brainres.2008.10.026
6. Hasan KM, Kamali A, Abid H, Kramer LA, Fletcher JM, Ewing-Cobbs L. Quantification of the spatiotemporal microstructural organization of the human brain association, projection and commissural pathways across the lifespan using diffusion tensor tractography. *Brain Struct Funct* 2010; **214**: 361–73. doi: https://doi.org/10.1007/s00429-009-0238-0
7. Hofer S, Frahm J. Topography of the human corpus callosum revisited—comprehensive fiber tractography using diffusion tensor magnetic resonance imaging. *Neuroimage* 2006; **32**: 989–94.
8. Alexander DC, Hubbard PL, Hall MG, Moore EA, Ptito M, Parker GJ, et al. Orientationally invariant indices of axon diameter and density from diffusion MRI. *Neuroimage*

2010; **52**: 1374–89. doi: https://doi.org/10.1016/j.neuroimage.2010.05.043
9. Barazany D, Basser PJ, Assaf Y. *In vivo* measurement of axon diameter distribution in the corpus callosum of rat brain. *Brain* 2009; **132**: 1210–20. doi: https://doi.org/10.1093/brain/awp042
10. Schneider T, Wheeler-Kingshott CA, Alexander DC. *In-vivo* estimates of axonal characteristics using optimized diffusion MRI protocols for single fibre orientation. *Med Image Comput Comput Assist Interv* 2010; **13**: 623–30.
11. Vicq d'Azyr F. Traité d'anatomie et de physiologie. Paris, France: Didot; 1786. Available from: (text) http://www.biusante.parisdescartes.fr/histmed/medica/cote?00519x01; (plates)http://www.biusante.parisdescartes.fr/histmed/medica/cote?00519x02
12. Bell C. The anatomy of the brain, explained in a series of engravings. London, UK: T.N. Longman and O. Rees, 1802. This image is © Wellcome Images, but has been altered into a Derivative Work by Christopher Wiggins by merging into the multiple image format and extraction of detail.
13. Dejerine J, Dejerine-Klumpke A. Anatomie des centres nerveux. Paris, France: Rueff; 1895. Available at: the Medical Heritage Library (http://www.archive.org/details/anatomiedescentr01dj).
14. Gray H. *Anatomy of the human body*. Philadelphia, USA: Lea & Febiger; 1918.
15. Schaltenbrand G, Wahren W. *Atlas for stereotaxy of the human brain*. 2nd edn. Stuttgart, Germany: Thieme; 1998.
16. Ludwig E, Klingler J. *Atlas cerebri humani*. Basel, Switzerland: S. Karger; 1956.
17. Duyn JH, van Gelderen P, Li TQ, de Zwart JA, Koretsky AP, Fukunaga M. High-field MRI of brain cortical substructure based on signal phase. *Proc Natl Acad Sci U S A* 2007; **104**: 11796–801. doi: https://doi.org/10.1073/pnas.0610821104
18. Schäfer A, Wharton S, Gowland P, Bowtell R. Using magnetic field simulation to study susceptibility-related phase contrast in gradient echo MRI. *Neuroimage* 2009; **48**: 126–37. doi: https://doi.org/10.1016/j.neuroimage.2009.05.093
19. Wiggins CJ, Gudmundsdottir V, Le Bihan D, Lebon V, Chaumeil M. Orientation dependence of white matter T2* contrast at 7 T: a direct demonstration. International Society for magnetic Resonance in medicine Scientific meeting and exhibition. 16th Annual Scientific Meeting; 2008 May 3–9. Toronto, Canada. Berkeley, USA: International Society for Magnetic Resonance in Medicine; 2008.
20. Marques JP, Maddage R, Mlynarik V, Gruetter R. On the origin of the MR image phase contrast: an *in vivo* MR microscopy study of the rat brain at 14.1 T. *Neuroimage* 2009; **46**: 345–52. doi: https://doi.org/10.1016/j.neuroimage.2009.02.023
21. Carmichael DW, Thomas DL, De Vita E, Fernández-Seara MA, Chhina N, Cooper M, et al. Improving whole brain structural MRI at 4.7 Tesla using 4 irregularly shaped receiver coils. *Neuroimage* 2006; **32**: 1176–84. doi: https://doi.org/10.1016/j.neuroimage.2006.04.191
22. Goense JB, Zappe AC, Logothetis NK. High-resolution fMRI of macaque V1. *Magn Reson Imaging* 2007; **25**: 740–7. doi: https://doi.org/10.1016/j.mri.2007.02.013
23. Thomas DL, De Vita E, Roberts S, Turner R, Yousry TA, Ordidge RJ. High-resolution fast spin echo imaging of the human brain at 4.7 T: implementation and sequence characteristics. *Magn Reson Med* 2004; **51**: 1254–64. doi: https://doi.org/10.1002/mrm.20106
24. Haase A, Frahm J, Matthaei D, Hänicke W, Merboldt KD. FLASH imaging: rapid NMR imaging using low flip-angle pulses. *J Magn Reson* 1986; **67**: 258–66. doi: https://doi.org/10.1016/0022-2364(86)90433-6
25. Li TQ, van Gelderen P, Merkle H, Talagala L, Koretsky AP, Duyn J. Extensive heterogeneity in white matter intensity in high-resolution T2*-weighted MRI of the human brain at 7.0 T. *NeuroImage* 2006; **32**: 1032–40. doi: https://doi.org/10.1016/j.neuroimage.2006.05.053
26. Reichenbach JR, Venkatesan R, Schillinger DJ, Kido DK, Haacke EM. Small vessels in the human brain: MR venography with deoxyhemoglobin as an intrinsic contrast agent. *Radiology* 1997; **204**: 272–7. doi: https://doi.org/10.1148/radiology.204.1.9205259
27. Wharton S, Schäfer A, Bowtell R. Susceptibility mapping in the human brain using threshold-based *k*-space division. *Magn Reson Med* 2010; **63**: 1292–304. doi: https://doi.org/10.1002/mrm.22334
28. Basser PJ, Mattiello J, LeBihan D. Estimation of the effective self-diffusion tensor from the NMR spin echo. *J Magn Reson B* 1994; **103**: 247–54. doi: https://doi.org/10.1006/jmrb.1994.1037
29. Fasano F, Bozzali M, Cercignani M, Hagberg GE. A highly sensitive radial diffusion measurement method for white matter tract investigation. *Magn Reson Imaging* 2009; **27**: 519–30. doi: https://doi.org/10.1016/j.mri.2008.08.005
30. Lohmann G, Bohn S, Müller K, Trampel R, Turner R. Image restoration and spatial resolution in 7-tesla magnetic resonance imaging. *Magn Reson Med* 2010; **64**: 15–22. doi: https://doi.org/10.1002/mrm.22488
31. Lazar M, Lee JH, Alexander AL. Axial asymmetry of water diffusion in brain white matter. *Magn Reson Med* 2005; **54**: 860–7. doi: https://doi.org/10.1002/mrm.20653
32. Zhang J, van Zijl PC, Mori S. Image contrast using the secondary and tertiary eigenvectors in diffusion tensor imaging. *Magn Reson Med* 2006; **55**: 439–49. doi: https://doi.org/10.1002/mrm.20767
33. Atkinson D, Batchelor PG, Clark CA. Track ribbons—visualising structural information in diffusion tensor axial asymmetry. International Society for magnetic Resonance in medicine Scientific meeting and exhibition, 15th Annual Scientific Meeting; 6–12 May 2007. Berlin, Germany. Berkeley, USA: International Society for Magnetic Resonance in Medicine; 2007.
34. Aboitiz F, Scheibel AB, Fisher RS, Zaidel E. Fiber composition of the human corpus callosum. *Brain Res* 1992; **598**: 143–53.
35. Yeatman JD, Ben-Shachar M, Bammer R, Feldman HM. Using diffusion tensor imaging and fiber tracking to characterize diffuse perinatal white matter injury: a case report. *J Child Neurol* 2009; **24**: 795–800. doi: https://doi.org/10.1177/0883073808331080
36. Frye RE, Hasan K, Xue L, Strickland D, Malmberg B, Liederman J, et al. Splenium microstructure is related to two dimensions of reading skill. *Neuroreport* 2008; **19**: 1627–31. doi: https://doi.org/10.1097/wnr.0b013e328314b8ee
37. Huang H, Zhang J, Jiang H, Wakana S, Poetscher L, Miller MI, et al. DTI tractography based parcellation of white matter: application to the mid-sagittal morphology of corpus callosum. *Neuroimage* 2005; **26**: 195–205. doi: https://doi.org/10.1016/j.neuroimage.2005.01.019
38. Pandya DN, Karol EA, Heilbronn D. The topographical distribution of interhemispheric projections in the corpus callosum of the rhesus monkey. *Brain Res* 1971; **32**: 31–43. doi: https://doi.org/10.1016/0006-8993(71)90153-3
39. Witelson SF. Hand and sex differences in the isthmus and genu of the human corpus callosum. A postmortem morphological study. *Brain* 1989; **112**: 799–835. doi: https://doi.org/10.1093/brain/112.3.799
40. Murre JM, Sturdy DP. The connectivity of the brain: multi-level quantitative analysis. *Biol Cybern* 1995; **73**: 529–45. doi: https://doi.org/10.1007/bf00199545
41. Adams DL, Sincich LC, Horton JC. Complete pattern of ocular dominance columns in human primary visual cortex. *J Neurosci*

2007; **27**: 10391–403. doi: https://doi.org/10.1523/jneurosci.2923-07.2007

42. Wedeen VJ, Rosene DL, Wang R, Dai G, Mortazavi F, Hagmann P, et al. The geometric structure of the brain fiber pathways. *Science* 2012; **335**: 1628–34. doi: https://doi.org/10.1126/science.1215280
43. Huang H, Xue R, Zhang J, Ren T, Richard LJ, Yarowsky P, et al. Anatomical characterization of human fetal brain development with diffusion tensor magnetic resonance imaging. *Neuroscience* 2009; **29**: 4263–73. doi: https://doi.org/10.1523/jneurosci.2769-08.2009
44. Denenberg VH, Kertesz A, Cowell PE. A factor analysis of the human's corpus callosum. *Brain Res* 1991; **548**: 126–32. doi: https://doi.org/10.1016/0006-8993(91)91113-f
45. Moses P, Courchesne E, Stiles J, Trauner D, Egaas B, Edwards E. Regional size reduction in the human corpus callosum following pre- and perinatal brain injury. *Cereb Cortex* 2000; **10**: 1200–10. doi: https://doi.org/10.1093/cercor/10.12.1200
46. Rajapakse JC, Giedd JN, Rumsey JM, Vaituzis AC, Hamburger SD, Rapoport JL. Regional MRI measurements of the corpus callosum: a methodological and developmental study. *Brain Dev* 1996; **18**: 379–88. doi: https://doi.org/10.1016/0387-7604(96)00034-4
47. Zhang H, Hubbard PL, Parker GJ, Alexander DC. Axon diameter mapping in the presence of orientation dispersion with diffusion MRI. *Neuroimage* 2011; **56**: 1301–15. doi: https://doi.org/10.1016/j.neuroimage.2011.01.084